Journal of Integrative Agriculture 2026, 25(7): 2739–2754

Available online at ScienceDirect

Journal of Integrative Agriculture



RESEARCH ARTICLE

SiTCD1 encodes a P-type PPR protein that affects early chloroplast development at low temperatures in foxtail millet

Zhilan Wang[1, 2*], Xiaofen Du[1, 2*], Kangni Han[2], Miao Li[1, 2], Shichao Lian[2], Yuxin Li[2], Yanfang Li[1, 2], Linyi Zhang[2], Xingchun Wang[1, 3#], Jun Wang[1, 2#]

[1] *College of Agriculture, Shanxi Agricultural University, Taigu 030800, China*
[2] *Houji Laboratory in Shanxi Province/Millet Research Institute, Shanxi Agricultural University, Changzhi 046011, China*
[3] *College of Life Sciences, Shanxi Agricultural University, Taigu 030800, China*

Highlights

- Temperature-sensitive chlorophyll-deficient 1 (*sitcd1*) foxtail millet plants exhibit reduced chlorophyll content, abnormal chloroplasts, and an albino phenotype during early leaf development at low temperatures.
- *SiTCD1* encodes a P-type PPR protein localized in chloroplasts that may participate in the splicing of plastid gene *atpF* at low temperatures.
- Accessions carrying the *SiTCD1*^{Hap2} allele are more tolerant to cold stress than those with the *SiTCD1*^{Hap1} allele at the bud bursting stage.

Abstract

Chloroplast gene expression relies on nucleus-encoded factors for RNA metabolic processing, but the mechanisms under cold stress remain poorly understood. In this study, we isolated and characterized a foxtail millet (*Setaria italica*) mutant, temperature-sensitive chlorophyll-deficient (*sitcd1*), which exhibited reduced chlorophyll content and abnormal chloroplasts, resulting in an albino phenotype during early leaf development at low temperatures (20°C during the day and 18°C at night, L20/D18). Map-based cloning revealed that *SiTCD1* encodes a P-type PPR protein localized in chloroplasts. In *sitcd1* background, transgenic lines overexpressing *SiTCD1* had nearly normal green leaves under L20/D18 conditions. *SiTCD1* was especially expressed in the earlier development of leaves at low temperatures. In addition, SiTCD1 bound directly to the plastid gene *atpF in vitro*, so it might participate in the splicing of plastid gene *atpF* at low temperatures. RNA-seq results indicated that the expression of genes related to metabolism (such as porphyrin, chlorophyll and glutathione metabolism), which require ATP for energy, was down-regulated in *sitcd1*, resulting in reductions in chlorophyll content, reduced glutathione (GSH), and its redox couple (GSH/oxidized glutathione (GSSG)) at low temperatures. As *sitcd1* exhibited greater sensitivity at the bud bursting stage than germination or the seedling stage under cold stress, we identified two haplotypes of *SiTCD1* (*SiTCD1*^{Hap1} and *SiTCD1*^{Hap2}) in 195 accessions, and found that accessions carrying the *SiTCD1*^{Hap2} allele were more tolerant to cold stress than those with the *SiTCD1*^{Hap1} allele at the bud bursting stage. In summary, our results suggest that *SiTCD1* is essential for early chloroplast development at low temperatures in foxtail millet.

Keywords: foxtail millet (*Setaria italica*), chloroplast development, *SiTCD1*, plastid gene *atpF*, low temperature

1. Introduction

Chloroplast development is an essential phase that allows seedlings to transition from heterotrophic to autotrophic growth, and it relies on the coordinated expression of nucleus-encoded polymerase (NEP) and plastid-encoded polymerase (PEP) genes (Liu *et al.* 2018; Li J Y *et al.* 2022). Although

Received 20 August 2024; Received in revised form 29 October 2024; Accepted 11 November 2024; Available online 18 December 2024
Zhilan Wang, Tel: +86-355-2204016, E-mail: wangyan11111ai@163.com; Xiaofeng Du, Tel: +86-355-2204016, E-mail: dxf6285210@126.com; [#]Correspondence Jun Wang, Tel/Fax: +86-355-2204158, E-mail: 128wan@163.com; Xingchun Wang, Tel/Fax: +86-354-6286908, E-mail: wxingchun@sxau.edu.cn
[*]These authors contributed equally to this study.

© 2026 CAAS. Publishing services by Elsevier B.V. on behalf of KeAi Communications Co. Ltd. This is an open access article under the CC BY-NC-ND license (http://creativecommons.org/licenses/by-nc-nd/4.0/). Peer review under responsibility of Editorial Board of *Journal of Integrative Agriculture*.
doi: 10.1016/j.jia.2024.12.022

considerable progress has been made in elucidating the molecular mechanisms of chloroplast development in plants (Zhang *et al.* 2021; Lan *et al.* 2023), the precise regulation of chloroplast gene expression in response to intracellular and environmental cues remains incompletely understood.

The chloroplast has been suggested to act as the central switch of plant responses to cold stress (Gao *et al.* 2022). Low temperature is a critical abiotic factor affecting chloroplast development, especially at the early stage of seedling greening (Wang Y F *et al.* 2016; Liu *et al.* 2021; Li J H *et al.* 2022; Li J Y *et al.* 2022). Sudden exposure to cold stress, which often occurs during early seedling development in the spring, inhibits seed germination and seedling survival, leading to reduced yield. Therefore, it is necessary to elucidate the molecular mechanisms involved in low-temperature stress on chloroplast development in crops including foxtail millet (*Setaria italica*). Temperature-sensitive and chlorophyll-deficient mutants have been invaluable for studying chloroplast development under cold stress in *Arabidopsis* (Wang S *et al.* 2016; Zhu *et al.* 2020; Okuzaki *et al.* 2021) and rice (Wang Y F *et al.* 2016; Cui *et al.* 2019; Liu *et al.* 2021). In foxtail millet, only three chlorophyll-deficient mutants have been identified: *striped leaf 1* (*sistl1*) (Tang *et al.* 2019), *sistl2* (Zhang *et al.* 2018) and *yellow-green leaf 1* (*siygl1*) (Li *et al.* 2016), and they exhibit yellow-green or striped leaves and abnormal chloroplasts. However, the specific genes involved in chloroplast development under cold stress in foxtail millet have not been identified.

Chloroplast RNAs must be processed to become functional mRNAs and rRNAs. This processing involves RNA-binding proteins that participate in various aspects of RNA metabolism, such as RNA cleavage, splicing, editing, and stabilization (Tillich and Krause 2010; Barkan 2011). Among these RNA-binding proteins, pentatricopeptide repeat (PPR) proteins play a crucial role in specific RNA processing pathways and significantly influence gene expression in chloroplasts (Chen *et al*. 2023; Lan *et al.* 2023). The PPR family consists of proteins characterized by tandem arrays of a repeated 35-amino acid motif and includes numerous members in land plants, with 450 in *Arabidopsis*, 477 in rice, and 486 in foxtail millet (Liu *et al.* 2016). Previous studies have demonstrated that some PPR proteins in plants respond to low-temperature environmental conditions. Specifically, chloroplast-localized PPR proteins such as CHLOROPHYLL DEFICIENT 4 (CDE4) (Liu *et al.* 2021), PALE-GREEN LEAF 12 (PGL12) (Chen *et al*. 2019), WHITE STRIPE LEAF (WSL) (Tan *et al.* 2014), WHITE STRIPE LEAF 4 (WSL4) (Wang *et al.* 2017), WHITE STRIPE LEAF 5 (WSL5) (Liu *et al.* 2018), and YOUNG LEAF WHITE STRIP (YLWS) (Lan *et al.* 2023) are involved in the splicing of various plastid transcripts, including *atpF*, *rpl2*, *rps12*, *ndhA*, and *ndhB*, during chloroplast development under low temperatures. Meanwhile, PPR proteins assist in the transcription and translation of genes encoding chloroplast ATP synthase, which consists of 26 peptides from nine different subunits, to produce ATP for the Calvin–Benson–Bassham (CBB) cycle and other energy-demanding processes (Gao *et al.* 2022). For example, PPR10 (Pfalz *et al.* 2009) and BIOGENESIS FACTOR REQUIRED FOR ATP SYNTHASE 2 (BFA2) (Zhang *et al.* 2019) regulate the stability of *atpH/F* mRNA, while ATP4 and SUPPRESSOR OF VARIEGATION 7 (SVR7) promote the translation of *atpB/E* mRNA in chloroplasts (Zoschke *et al.* 2012). Loss-of-function mutations of these proteins result in a specific reduction of chloroplast ATP synthase. However, the mechanism by which PPR proteins regulate chloroplast ATP synthase-related genes under cold stress remains to be elucidated.

In this study, we isolated a foxtail millet mutant, temperature-sensitive chlorophyll-deficient (*sitcd1*), with an albino phenotype during early leaf development under low-temperature conditions. Positional cloning revealed that *SiTCD1* encodes a P-type PPR protein that was localized to the chloroplasts. Verification of *SiTCD1* overexpression confirmed that transgenic lines had nearly normal green leaves under 20-h-light/18-h-dark (L20/D18) conditions in the *sitcd1* background. Furthermore, REMSAs assays demonstrated that SiTCD1 binds directly to the plastid gene *atpF in vitro*, and participates in the splicing of plastid gene *atpF* under low temperatures. RNA-seq and qRT-PCR analyses showed that the genes related to metabolic pathways essential for ATP energy production are significantly downregulated in *sitcd1* at low temperatures. Given those findings, a haplotype analysis of *SiTCD1* indicated that the $SiTCD1^{Hap2}$ allele is more tolerant to cold stress than the $SiTCD1^{Hap1}$ allele at the bud bursting stage. Thus, this study elucidated the role of *SiTCD1* in regulating early chloroplast development in foxtail millet under low-temperature conditions.

2. Materials and methods

2.1. Plant materials, temperature conditions, agronomic traits, and photosynthetic characteristics

The spontaneous mutant *sitcd1* was identified from 'Changnong 35' (wild type, WT), a foxtail millet cultivar. Four segregating F_2 populations derived from the crosses '*sitcd1*×Changnong 35', 'Changnong 35×*sitcd1*', '*sitcd1*×09K65 (another cultivar)', and '*sitcd1*×Pinzi39 (a third cultivar)' were used for genetic analysis (Appendix A). The F_2 population derived from the '*sitcd1*×Pinzi39' cross was used for gene mapping. Agriculturally important traits were assessed during the harvest period. Net photosynthetic rate (P_n), stomatal conductance (G_s), intercellular CO_2 concentration (C_i), and transpiration rate (T_r) were measured on the first, fully expanded leaf using a CIRAS-2 Portable Photosynthesis System (LI-COR, Nebraska, USA) at the seedling, jointing, and heading stages. Each sample was analyzed in three biological replicates.

WT and *sitcd1* plants were grown in an artificial climate chamber with a 10-h-light/14-h-dark photoperiod under day/night temperature cycles of either 30°C/28°C, 25°C/23°C, or 20°C/18°C (referred to as L30/D28, L25/D23, or L20/D18, respectively). In addition, WT and *sitcd1* seeds were sown in fields in mid-April, mid-May, and late June, with spikes reaching the heading stage in mid-July (mean temperature of 25.9°C), early August (mean temperature of 22.8°C), and early September (mean temperature of 17.5°C), respectively.

2.2. Chlorophyll content, microscopic observations, and transmission electron microscopy

Chlorophyll content was determined according to a method described previously (Arnon 1949). Leaves from seedlings at the three-leaf stage and the glumes of panicles at the heading stage were collected from *sitcd1* and WT in the fields, and the leaves of *sitcd1* and WT seedlings at the three-leaf stage of plants grown in an incubator at different temperatures were collected with three biological replicates. Approximately 0.1 g fresh tissue was immersed in 95% (v/v) ethanol for 48 h in the dark. The absorbance of the extracts was then measured with a 722s ultraviolet/visible spectrophotometer (Shimadzu, Shanghai, China) at 470, 649, and 665 nm.

The third leaf veins of WT and *sitcd1* plants grown in the fields were observed and photographed with a universal biological microscope BX51 (Olympus, Japan).

Chloroplast structures of the third leaves from *sitcd1* and WT plants grown at different temperatures in an incubator were examined using an H-7800 type TEM (Hitachi, Japan).

2.3. Map-based cloning of *SiTCD1* and plant transformation

A total of 788 molecular markers distributed across the genome (Jia *et al.* 2009; Zhang *et al.* 2014; Fang *et al.* 2016) were used to assess the genetic background of *sitcd1*. For genetic analysis, four segregating F_2 populations were produced from the crosses mentioned above. The F_2 population developed from the cross of '*sitcd1*×Pinzi39' was used to performed BSA-seq analysis to isolate the genomic regions responsible for the mutations in *sitcd1*. Two DNA pools, namely a green pool (G-pool) and a white-striped pool (W-pool), consisted of equal amounts of genomic DNA extracted from 50 F_2 individuals showing the most extreme green leaf or white-striped phenotype, respectively. The G-pool, W-pool, and two parental lines (*sitcd1* and Pinzi39) were subjected to next generation sequencing separately, with a sequencing depth of ~20× for the two parents and ~30× in each bulk, on an Illumina HiSeq 2500 System using the standard protocol (BMK, Beijing, China). After the barcodes were trimmed, clean, high-quality reads from each sample were mapped onto the 'Yugu 1' foxtail millet reference genome in Burrows Wheeler Aligner (Li *et al.* 2009). The SNP set was formed by combining GATK (Mckenna *et al.* 2010) and Samtools (Li and Durbin 2009) SNP calling analysis with default parameters. SNPs identified between the pools were regarded as polymorphic for the association studies. Next, the ΔSNP-index (Abe *et al.* 2012) and Euclidean distance (ED) were calculated. Regions above the threshold were considered as trait-related candidate regions.

A total of 1,393 F_2 individuals derived from '*sitcd1*×Pinzi39' were selected for fine-mapping of the *SiTCD1* locus. Molecular markers with nucleotide polymorphisms between *sitcd1* and Pinzi39 were used to identify markers tightly linked to *SiTCD1*.

For complementation of *sitcd1*, the full-length (2,253 bp) cDNA of *SiTCD1* was cloned into the pCAMBIA1300 vector backbone downstream of the *Ubi* promoter, yielding the vector pBWA(V)HU. The resulting construct was transformed into *sitcd1* by the *Agrobacterium*-mediated method with *Agrobacterium tumefaciens* (strain EHA105) (Yang *et al.* 2020). Hygromycin-resistant calli were grown in a greenhouse to obtain transgenic plants and their seeds. The presence of the target gene and genomic background in positive plants were further verified by PCR analysis.

2.4. RNA isolation, RT-PCR, and qRT-PCR analyses

Total RNA was extracted with TRIzol reagent (TaKaRa, 9108, Dalian, China) and reverse-transcribed into first-strand cDNA using the PrimeScript™ 1st Strand cDNA Synthesis Kit (TaKaRa, 6110A). Real-time quantitative PCR (qRT-PCR) was performed using the TB Green Premix *Ex Taq* II Kit (TaKaRa, RR820A) on a CFX96 Real-time PCR System (Bio-Rad, Dalian, China), and *SiACTIN7* (*Seita.7G294000*) was selected as the internal reference gene. Three biological replicates were performed for each experiment, and the relative expression level of each gene was calculated by the $2^{-\Delta CT}$ method.

2.5. Subcellular localization

The coding sequence of *Green fluorescent protein* (*GFP*) was introduced into the multiple cloning sites of pCAMBIA1301 to generate vector pBWA(V)HS-GFP. Subcellular localization was assessed by cloning the full-length coding sequence of *SiTCD1* in-frame and upstream of the *GFP* gene sequence, under the control of the cauliflower mosaic virus (CaMV) 35S promoter, yielding *35S:SiTCD1-GFP*. The coding sequence corresponding to *sitcd1* (aa 69–750) was also cloned in the same vector, generating *35S:sitcd1-GFP*, as contained the sequence encoding the putative cTP domain of SiTCD1, resulting in *35S:cTP_82aa_SiTCD1-GFP*. The resulting constructs and empty vector were transfected into rice protoplasts (cultivar 9311) extracted from 9-d-old seedlings and incubated at 28°C for 16 h in darkness before examination (Chen *et al.* 2006). GFP fluorescence was observed with a confocal laser microscope (Nikon C2-ER, Japan).

2.6. RNA splicing analysis of chloroplast transcripts

To assess whether SiTCD1 is involved in the RNA splicing of plastid genes, we analyzed the chloroplast genome sequence of foxtail millet available in the NCBI database (http://www.ncbi.nlm.nih/nuccore/NC_02285.1/). The plastid genes with introns were selected. Accordingly, all chloroplast transcripts with group II introns were amplified using primers flanking the introns (except for *rps12* due to its long intron) *via* semi-quantitative Real-Time PCR, followed by agarose gel electrophoresis to estimate splicing efficiency. For RNA splicing efficiency analysis by qRT-PCR, specific primers located in intron-exon (as unspliced forms) and exon–exon (as spliced forms) links were designed (Appendix B).

2.7. RNA electrophoresis mobility shift assays (REMSAs)

The truncated coding sequence of *SiTCD1* (encoding aa 69–750) was cloned in-frame with the sequence of a His tag in vector pET28a-SUMO. Protein production in *Escherichia coli* strain BL21(DE3) was induced by treatment with 0.2 mmol L^{-1} isopropyl-β-D-thiogalactopyranoside (IPTG) at 16°C for 16 h (OD_{600}=0.6–0.8). The His-SUMO fused protein was

purified with Ni-NTA beads (SA005100; Smart-Lifesciences). The RNA probes were chemically synthesized, and their 5′ ends were labeled with Cy5 (Sangon Biotech (Shanghai) Co., Ltd., China). The corresponding unlabeled probes were also chemically synthesized for competition assays. For REMSA, the RNA probes and recombinant His-SUMO-SiTCD1$^{69–750}$ protein were incubated at room temperature for 30 min in a reaction solution (1 mmol L^{-1} $MgCl_2$, 10 mmol L^{-1} HEPES, pH 7.3, 20 mmol L^{-1} KCl, 5% (v/v) glycerol, 0.1 μg tRNA, and 1 mmol L^{-1} dithiothreitol). The reactants were separated by electrophoresis in a native PAGE gel, and signals were detected using an Azure Biosystems C600 Imager.

2.8. RNA sequencing (RNA-seq) analysis

Total RNA was independently extracted from the seedling leaves from WT, *sitcd1* and *SiTCD1*-OE plants grown in an artificial climate chamber at L30/D28 or L20/D18 with three biological replicates. Construction of the sequencing libraries, quality control, and paired-end sequencing were performed on an Illumina HiSeq platform by Biomarker Technologies (Beijing, China). With the adapters and low-quality reads removed, the resulting clean reads were mapped separately to the 'Yugu 1' foxtail millet reference genome using HISAT2 software (http://daehwankimlab.github.io/hisat2/). The significance of differentially expressed gene (DEG) expression was determined using criteria of abs[$\log_2$(fold-change)]>1.0 and false discovery rate (FDR)<0.01. The unigenes were compared to public databases (Non-Redundant Protein Sequence Database (NR), Gene Ontology (GO), Kyoto Encyclopedia of Genes and Genomes (KEGG), Eukaryotic Orthologous Groups (KOG), Clusters of Orthologous Groups (COG), and Protein family database (Pfam)) using BLAST with an e-value threshold of 10^{-5}.

2.9. Measurement of physiological indicators

The contents of adenosine triphosphate (ATP), soluble sugar content (SSC), reduced glutathione (GSH), and oxidized glutathione (GSSG) were determined as previously described (Beutler and Mathai 1967; Alpert and Gilbert 1985; Buysse and Merckx 1993). The activities of the glutathione reductase (GR), superoxide dismutase (SOD), peroxidase (POD), and catalase (CAT) enzymes were determined as previously described (Demiral and Türkan 2005). $O_2^{-}\cdot$ in the leaf was detected using nitro blue tetrazolium (NBT) according to the method described previously (Zhao *et al.* 2018).

2.10. Natural variation of *SiTCD1* in foxtail millet

The genomic sequence of *SiTCD1* (including the promoter) was analyzed in a 110 *Setaria* pan-genome, which was an assembly of 110 representative genomes from a worldwide collection (He *et al.* 2023). Molecular markers, developed according to the detected variation, were used to conduct a haplotype analysis of *SiTCD1* across 195 accessions from natural populations (141 Chinese landraces, 47 modern cultivars, and 7 worldwide landraces) (Li *et al.* 2022). The cold tolerance levels at the bud bursting stage of the 195 accessions were assessed in an incubator. Specifically, seeds were placed in an oven at 45°C for 24 h to break seed dormancy. The seeds were disinfected with 50% (w/v) sodium hypochlorite solution and rinsed with sterile water five times. Next, the seeds were soaked in water and allowed to germinate for 24 h in a Petri dish with two sheets of filter paper. Thirty seeds with 2 mm coleoptile lengths were selected and placed on hydroponic plates with Yoshida solution for cultivation at 25°C for 36 h in darkness. Afterward, the hydroponic plates of control materials were kept in an incubator set to 28°C/22°C temperature cycles and a 14-h-light/10-h-dark photoperiod. For cold treatment, the hydroponic cassettes were placed in a growth incubator set to 6°C under a 14-h-light/10-h-dark photoperiod for 3 d. After cold treatment, the hydroponic plates were returned to control conditions in an incubator and allowed to recover for 7 d. The scoring scale comprised five levels: 4, dark green leaf and rapid growth; 3, light green leaf, good growth and slow development; 2, less green leaf, slow growth and slower development; 1, deformed seedlings and arrested development; and 0, dead buds. The cold tolerance level during the budding stage was calculated based on the formula: (0×Number of plants at level 0+1×Number of plants at level 1+2×Number of plants at level 2+3×Number of plants at level 3+4×Number of plants at level 4)/30. A correlation analysis between cold tolerance level and haplotypes was conducted. Differences in phenotypic values and haplotypes were examined using the Student's *t*-test.

3. Results

3.1. Phenotypic characterization of the *sitcd1* mutant

The mutant *sitcd1* was identified from a spontaneous mutant derived from Changnong 35, a foxtail millet cultivar. *sitcd1* seedlings before the fifth-leaf stage (L5) produced white-striped leaves (Fig. 1-A), which then became green from the L5 stage in the field, and there was no significant difference in leaves compared to WT at the jointing stage (Appendix C). Meanwhile, the immature *sitcd1* panicle was not fully green at the heading stage, in contrast to WT (Fig. 1-B).

Consistent with the striped phenotype observed in *sitcd1*, the contents of chlorophyll *a* (Chl *a*), Chl *b*, and carotenoids in the striped leaves of *sitcd1* seedlings were significantly lower than those in WT. Similarly, the pigment contents were significantly lower in the glumes of young *sitcd1* panicles compared to WT at the heading stage (Appendix C). In WT, mature vascular bundles were surrounded by a layer of large circular or oval bundle sheath cells and an outer layer of spindly mesophyll cells, and two or three mesophyll cell layers were observed around the bundle sheath cells of two adjacent Kranz structures. By contrast, *sitcd1* had abnormal Kranz structures that lacked bundle sheath cells surrounding the vascular bundles with few chloroplasts, and some individual vascular tissues were underdeveloped (Fig. 1-C).

The photosynthetic properties showed that the C_i of *sitcd1* was significantly higher than that of WT at the seedling stage, while the G_s and P_n values of *sitcd1* were lower than those of WT at the seedling and jointing stages, but higher than those of WT at the heading stage (Appendix C).

In addition, the values for agriculturally important traits (e.g., panicle diameter, panicle weight, grain weight and

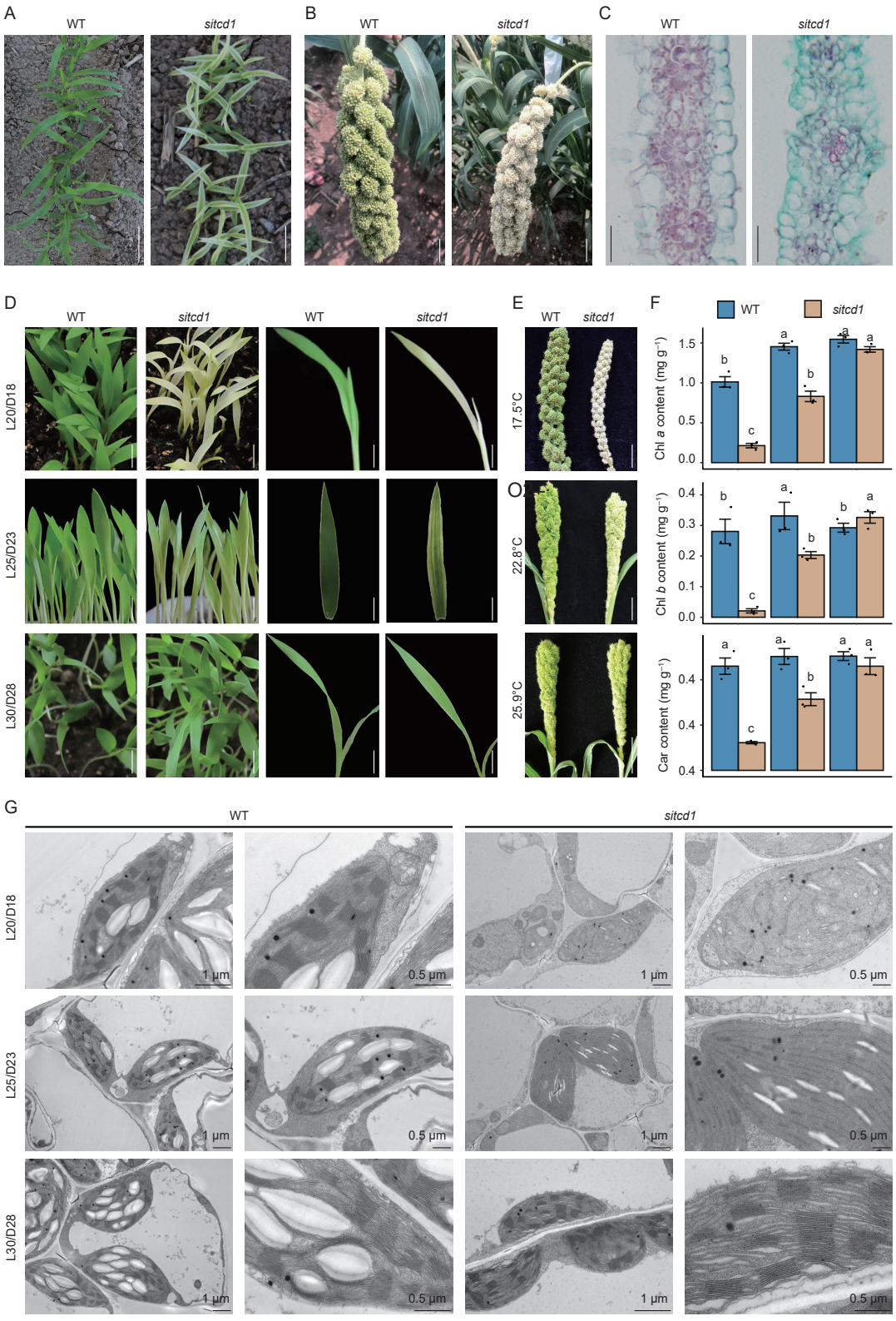


Fig. 1 Phenotypes of *sitcd1*. A, phenotypes of wild type (WT) and *sitcd1* seedlings 3 wk after planting in the field. Bar=2 cm. B, panicle phenotypes of WT and *sitcd1* at the flowering stage in the field. Bar=3 cm. C, vascular bundles of WT and *sitcd1* third-leaf fragments in resin-embedded sections. Bar=100 μm. D, leaves of WT and *sitcd1* seedlings in a growth chamber under L20/D18, L25/D23, and L30/D28 conditions. L20/D18, L25/D23, and L30/D28, light/dark temperatures of 20°C/18°C, 25°C/23°C, and 30°C/28°C, respectively. Bar=1 cm. E, the panicles of *sitcd1* were albino in early September (corresponding to a mean temperature of ~17.5°C), but light green in early August (mean temperature of ~22.8°C), and appeared to accumulate as much chlorophyll as WT panicles in mid-July (mean temperature of ~25.9°C). Bar=3 cm. F, leaf pigment concentrations of WT and *sitcd1* at the three-leaf stage in a growth chamber under L20/D18, L25/D23 and L30/D28 conditions. Chl, chlorophyll; Car, carotenoids. Bars mean SD (n=3). Letters indicate significant differences (P<0.05, one-way ANOVA, Duncan's test). G, transmission electron micrographs of mesophyll cells from WT and *sitcd1* seedling leaves under L20/D18, L25/D23 and L30/D28 conditions.

seed-setting rate) were significantly lower in *sitcd1* than in WT (Appendix D).

3.2. The *sitcd1* plants had an albino phenotype with defective chloroplast development at low temperatures

The *sitcd1* seedlings exhibited an albino phenotype with severely reduced chlorophyll contents under L20/D18, white-striped leaves with moderately lower chlorophyll contents under L25/D23, and green leaves with no significant differences in chlorophyll contents compared to WT under L30/D28 (Fig. 1-D and F). In addition, the accumulation of chlorophyll in glumes from young panicles was limited under lower temperatures but almost normal at higher temperatures in the field (Fig. 1-E).

The ultrastructural features of chloroplasts showed that most mesophyll cells in *sitcd1* were irregular in shape and their organelle structure was abnormal under L20/D18, with the plastids failing to develop into chloroplasts with a stacked thylakoid structure; the mesophyll cells developed normal chloroplasts under L25/D23, with fewer scattered grana lamellae in the thylakoid lamellae compared to *sitcd1* in L20/D18; and the mesophyll cells under L30/D28 had well-developed chloroplasts similar to WT (Fig. 1-G). Therefore, *sitcd1* showed defective chloroplast development at low temperatures, consistent with its visible phenotype and reduced chlorophyll contents.

3.3. Map-based cloning of the *SiTCD1* gene

The genetic background analysis results indicated that *sitcd1* has 98.97% consistency with WT. Furthermore, genetic analysis showed that all four derived F_2 populations showed 3:1 segregation ratios for the green-to-albino phenotype, indicating that the albino phenotype of *sitcd1* is controlled by a single recessive nuclear gene (Appendix A).

The *sitcd1* locus was identified with an F_2 population derived from the cross '*sitcd1*×Pinzi39'. First, the *sitcd1* locus was mapped to a 3.03 Mb region (1,132,000–14,350,000) on Chr. 9 using BSA-seq (Appendix E). On that basis, the *sitcd1* locus was finally delimited to a 19.78 kb region between markers *MRI607* and *MRI844* (Fig. 2-A). This region harbors four open reading frames (ORF) (Fig. 2-B) (Appendix F). Sequence analysis identified a 189 bp deletion in the 5′ untranslated region (UTR) and the first exon of ORF1 (*Seita.9G185600*) in *sitcd1*, leading to a start translation from the new starting codon (+205 bp) to produce a 68-amino acid deletion protein (Fig. 2-C).

To verify whether the 189 bp deletion of *Seita.9G185600* was responsible for the *sitcd1* phenotype, the full-length (2,253 bp) WT cDNA of *Seita.9G185600* was transformed into *sitcd1*. All three positive transgenic lines (*SiTCD1*-OE1, *SiTCD1*-OE2 and *SiTCD1*-OE3) had nearly normal green leaves under L20/D18 conditions (Fig. 2-D), and the expression of *SiTCD1* was significantly increased in all transgenic lines (Fig. 2-G).

SiTCD1 was predicted to be a P-type PPR protein, with 17 tandem repeat PPR motifs (Appendix G), and SiTCD1 is homologous to rice YSA (*Os03g40020*, with 91.3% identity) (Su *et al.* 2012) and *Arabidopsis* MEE40 (At3g53700, with 74.7% identity) (Zybailov *et al.* 2018) (Appendix H). These results indicated that *SiTCD1* encodes a previously uncharacterized PPR protein which is crucial for chloroplast development under low temperature conditions in foxtail millet.

3.4. *SiTCD1* was mainly expressed in earlier leaves at low temperatures

To gain insight into the expression pattern of *SiTCD1* in WT plants, qRT-PCR was performed on various tissues. The results showed that *SiTCD1* was constitutively expressed in both vegetative and reproductive tissues, including leaves, stems, panicles, and roots. Moreover, the data also showed that the *SiTCD1* transcript preferentially accumulated in earlier leaves, stems and panicles, especially earlier seedling leaves (Appendix I). Next, the *SiTCD1* expression levels in different leaves of a seedling plant were investigated, and the highest expression was detected in the first leaf (L1) (Fig. 2-E and F). Moreover, *SiTCD1* transcription levels in the leaves of all material seedlings (WT, *sitcd1*, *SiTCD1*-OE1, *SiTCD1*-OE2, and *SiTCD1*-OE3) were significantly higher at lower temperatures (Fig. 2-G). These results indicated that *SiTCD1* transcription accumulates in earlier leaves at low temperatures.

3.5. SiTCD1 was localized to the chloroplast

Using the two online prediction servers Chloro P (http://www.cbs.dtu.dk/services/Chloro P/) and Target P (http://www.cbs.dtu.dk/services/Target P/), the first 50–60 amino acids (aa) at the N terminus of SiTCD1 was predicted to be a putative plastid transit peptide. The subcellular localization was evaluated by fusing GFP to the N terminus of SiTCD1 to produce three constructs: WT (35S:SiTCD1-GFP), mutated forms (35S:sitcd1-GFP), and the cTP-encoding domain of SiTCD1 (35S:cTP_82aa_SiTCD1-GFP) (Fig. 2-H). GFP fluorescence was detected in the chloroplasts transfected with *35S:SiTCD1-GFP* or *35S:cTP_82aa_SiTCD1-GFP*, but not with *35S:sitcd1-GFP* (Fig. 2-I). We concluded that the sitcd1 protein was not targeted to chloroplasts. The co-localization of SiTCD1 with mitochondrial OsMST markers yielded no localization signal for SiTCD1 in mitochondria (Appendix I). These results indicated that SiTCD1 is a chloroplast-localized protein.

3.6. *SiTCD1* gene might be involved in *atpF* splicing at low temperatures

Since P-type PPR proteins in plants are required for RNA splicing (Barkan and Small 2014; Liu *et al.* 2021; Zhang *et al.* 2021; Lan *et al.* 2023), we tested whether SiTCD1 is involved in the RNA splicing of plastid genes. An analysis of the chloroplast genome of foxtail millet revealed 16 group II introns and one group I intron. The group I intron was in plastid gene *trnL*, while the group II introns were present in plastid genes *atpF*, *ndhA*, *ndhB*, *petB*, *petD*, *rpl2*, *rpl16*, *rps12*, *rps16*, *trnA*, *trnK*, *trnI*, and *trnV* with one intron each, and *rps12* and *ycf3* with two introns each. The lengths of the amplified transcript products for all the plastid genes with group II introns (except for *rps12* due to its long intron) were

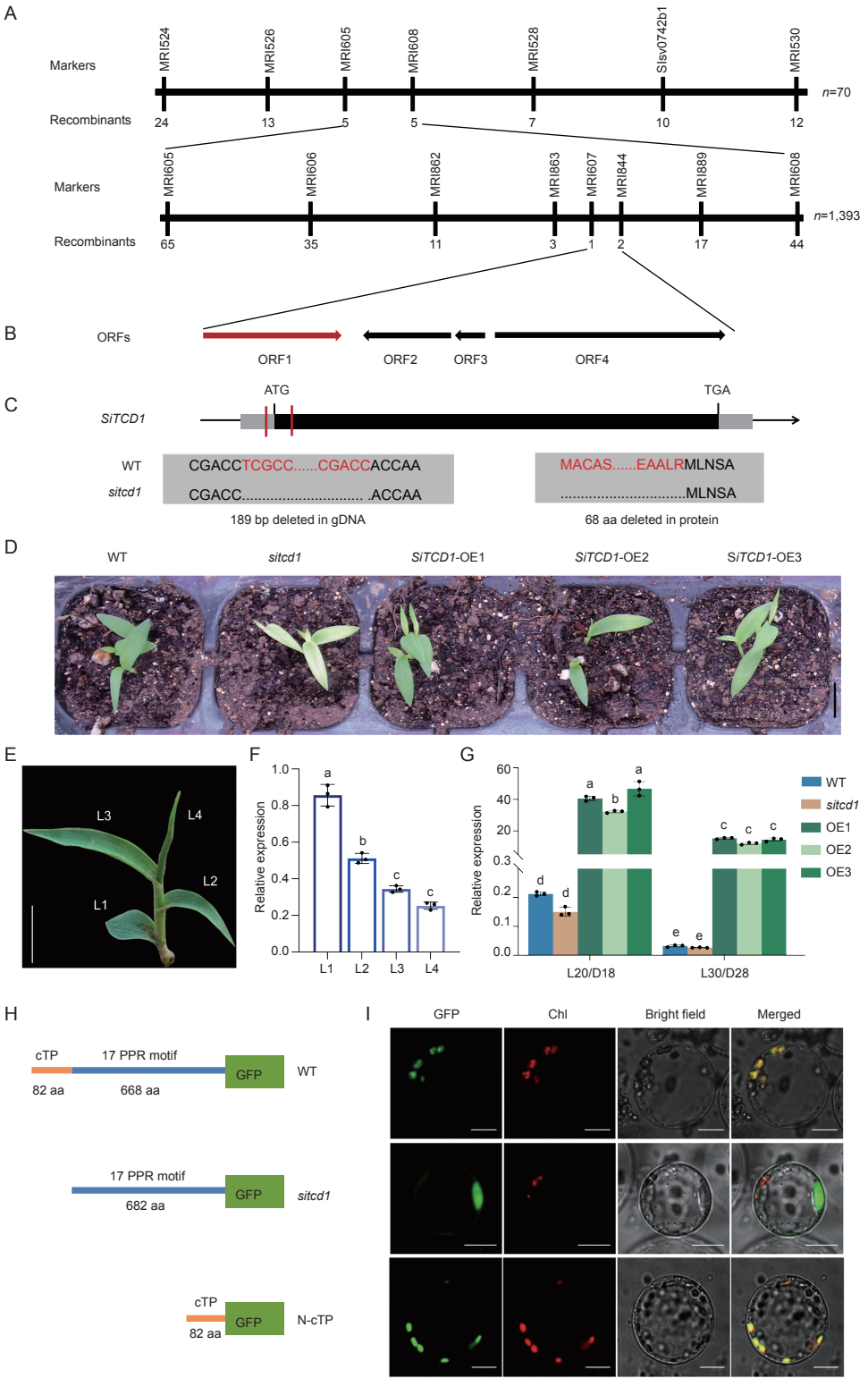


Fig. 2 Map-based cloning, expression pattern analysis and subcellular localization of *SiTCD1*. A, the *SiTCD1* locus narrowed down to a 19.78 kb region between markers MRI607 and MRI844. B, four predicted open reading frames (ORFs) in the mapped region. C, gene structure of *SiTCD1* (ORF1). Black boxes represent exons; grey boxes indicate the 5′- and 3′-untranslated regions (UTRs). A 189 bp deletion in 5′-UTR and the exon of ORF1 (*Seita.9G185600*) in the *sitcd1* led to a 68 amino acid deletion in the encoded protein. D, phenotypes of wild type (WT), *sitcd1*, *SiTCD1*-OE1, *SiTCD1*-OE2, and *SiTCD1*-OE3 (*sitcd1* overexpressing *SiTCD1*) at the seedling stage at low temperatures. Bar=1 cm. E and F, *SiTCD1* expression levels in different leaves of young seedlings. L1 to L4 indicate the first to the fourth leaves. Bar=1 cm. G, *SiTCD1* expression levels in seedlings of WT, *sitcd1* and overexpression lines (OE1, OE2, and OE3) under light/dark temperatures of 20°C/18°C and 30°C/28°C (L20/D18 and L30/D28) conditions. Bars are SD (n=3). Letters indicate significant differences (P<0.01, one-way ANOVA, Duncan's test). H and I, SiTCD1-GFP, sitcd1-GFP and cTP-GFP (82 amino acid fragment in the N terminus of SiTCD1) fusion proteins transiently expressed in protoplasts. The red signal is chloroplast autofluorescence. Bars=10 μm.

comparable between WT and *sitcd1* under L20/D18 and L30/D28 conditions. Interestingly, unspliced RNA precursors for the ATP synthase CF_0 subunit I gene *atpF* were detected in *sitcd1* but not in WT under L20/D18 conditions (Fig. 3-A). The transcript abundance of *atpF-S*, the fully spliced form of *atpF*, was markedly lower in *sitcd1*, whereas that of *atpF-U*, the unspliced form of *atpF*, was higher in *sitcd1* compared to the WT and transgenic lines (*SiTCD1*-OE1, *SiTCD1*-OE2, and *SiTCD1*-OE3) under L20/D18 conditions (Fig. 3-B). More importantly, comparable patterns for *atpF-S* and *atpF-U* were detected in all materials under L30/D28 conditions (Fig. 3-C and D). These results indicated that SiTCD1 might regulate the RNA splicing of *atpF* at low temperatures.

3.7. SiTCD1 modularly recognized and bound to *atpF* transcripts *in vitro*

Bioinformatics analysis showed that SiTCD1 contains 17 PPR domains (Appendix G). The specific sequence recognized by SiTCD1 was predicted based on the PPR code (Yan *et al.* 2019) with RPISeq (http://pridb.gdcb.iastate.edu/RPISeq/) (Appendix J). This analysis defined the predicted binding sequence of SiTCD1 as (?) (–) (U>C>G) (U>C>G) (A>G) (U>C>G) (U>C>G) (U>C>G) (U>C>G) (U>C>G) (C>U>A) (C>U) (U>C>G) (U>C>G) (C) (U>C>G) (?) (Fig. 4-A). Notably, the 8 nt sequence UUUUUCUU was detected in the intron of the *atpF* transcript, and 35 nucleotides including the 8 nt (UUUUUCUU) of *atpF* were prepared and designated as the *atpF*-probe (Fig. 4-B). This REMSA results showed that the complexes of His-SUMO-

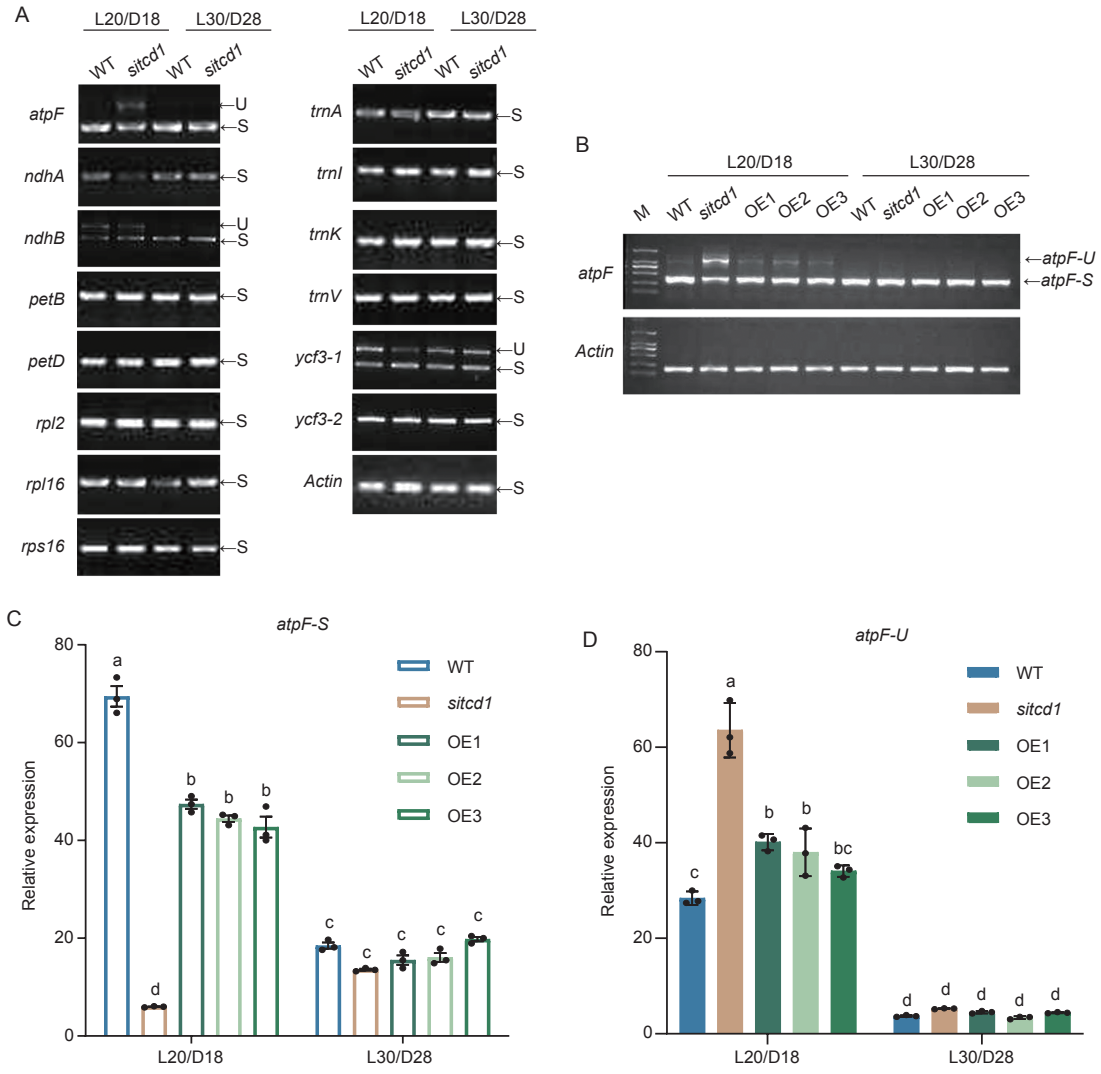


Fig. 3 *SiTCD1* is required for RNA splicing of the plastid gene *atpF* at low temperatures. A, splicing analysis of all transcripts from foxtail millet chloroplast genes containing introns (except for *rps12* due to its long intron) in the wild type (WT) and *sitcd1* third-leaf-stage seedlings under light/dark temperatures of 20°C/18°C and 30°C/28°C (L20/D18 and L30/D28) conditions, performed using RT-PCR. Spliced (S) and unspliced (U) transcript bands are indicated on the right. B, RT-PCR analysis of the *atpF* transcripts of the WT, *sitcd1* and overexpression lines (OE1, OE2, and OE3) in third leaf-stage seedlings under L20/D18 and L30/D28 conditions. The product of the spliced *atpF* transcripts (*atpF-S*) had an expected size of 337 bp, and the unspliced transcripts (*atpF-L*) were 1,207 bp. Molecular weight markers (M) are shown on the left. C and D, *AtpF-S* and *AtpF-U* expression levels in seedlings of WT, *sitcd1* and overexpression lines (OE1, OE2, and OE3) under L20/D18 and L30/D28 conditions. Bars mean SD (n=3). Letters indicate significant differences (P<0.01, one-way ANOVA, Duncan's test).

SiTCD1$^{69–750}$ and the RNA probes of *atpF* migrated more slowly, and the binding intensity decreased with an increasing concentration of unlabeled competitors (Fig. 4-C and D). The negative control showed no retarded band when using a probe specific to *ndhA* (Fig. 4-E). These results demonstrated that SiTCD1 binds directly to the *atpF* transcript *in vitro*.

3.8. Metabolic pathways required for ATP energy are significantly different in *sitcd1* at low temperatures

To investigate the sensitivity of *sitcd1* to temperature, transcriptome analysis was performed on the *sitcd1*, WT and transgenic lines under different temperatures. First, the transcription levels of plastid genes were analyzed under L20/D18 conditions. The level of spliced *atpF* transcript was much lower than the transcripts from other plastid genes with the group II intron, and the levels of transcripts transcribed by PEP decreased, including *psaA*, *psaB*, *psaJ*, *psbB*, and *psbC*, while the levels of transcripts transcribed by NEP increased, including *rpoA*, *rpoB*, *rpoC1*, and *rpoC2* in *sitcd1* (Appendix K). Next, under the

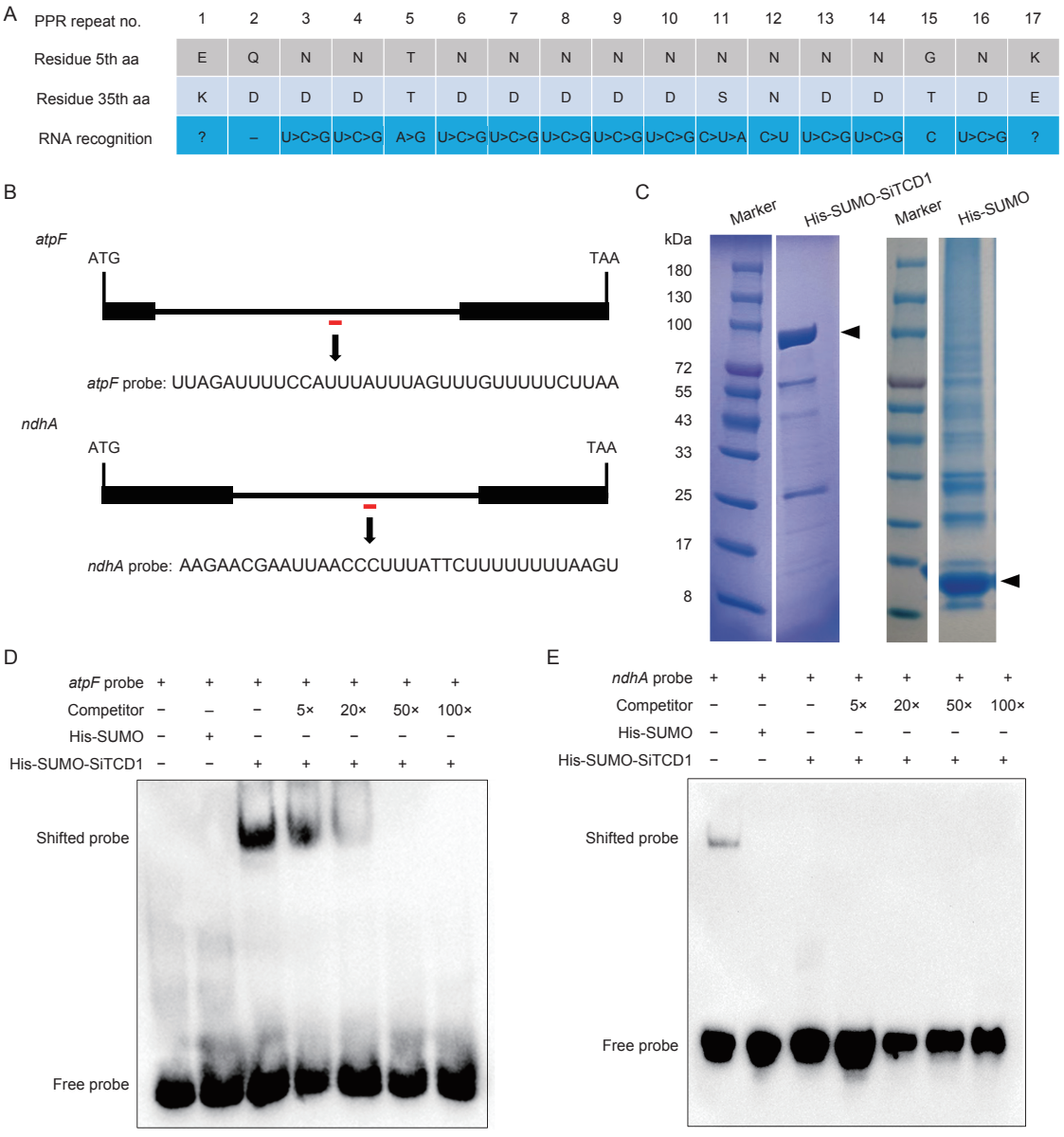


Fig. 4 Predicted nucleotides targeted by the PPR motifs and RNA electrophoretic mobility shift assay (REMSA) of SiTCD1. A, 17 predicted nucleotides targeted by the 17 PPR motifs. In each repeat, the amino acid residues at positions 5 and 35 and their nucleotide targets are shown. A dash (–) represents no correlated RNA bases for that PPR code identified by biochemical assays (EMSA, ITC); a question mark (?) represents unknown bases, as no biochemical assays were performed to identify the correlated RNA bases for the PPR code. B, schematic sequences of RNA probes, showing the REMA probes (red) in *atpF* and *ndhA*. The *ndhA* probe was used as a negative control. C, purified recombinant His-SUMO-SiTCD1$^{69–750}$ and His-SUMO separated by SDS-PAGE. D and E, REMSA of His-SUMO-SiTCD1$^{69–750}$ with the *atpF* and *ndhA* RNA probes. The *atpF* and *ndhA* RNA probes were biotinylated and incubated with purified His-SUMO or His-SUMO-SiTCD1$^{69–750}$ fusion proteins. Unlabeled probe was used as a competitor. Increasing amounts of His-SUMO-SiTCD1$^{69–750}$ and unlabeled competitors were used to determine the dose dependence and competitiveness of the binding.

L20/D18 treatment, 9,331 differentially expressed genes (DEGs) were identified between WT and *sitcd1*, as well as 8,614 DEGs between *SiTCD1*-OE and *sitcd1*, but only 778 DEGs were found between WT and *SiTCD1*-OE (Fig. 5-A). KEGG pathway analysis indicated that the expression of genes related to "starch and sucrose metabolism", "carbon metabolism", "porphyrin and chlorophyll metabolism", "glutathione metabolism", and "glycine, serine and threonine metabolism" were dramatically different in *sitcd1* relative to WT and *SiTCD1*-OE (Fig. 5-B). Nevertheless, under L30/D28 conditions, far fewer DEGs were found in the same three pairwise comparisons, ranging from 218 to 356. KEGG pathway analysis indicated that the expression levels of genes related to secondary metabolism, such as flavonoid, zeatin, carotenoid, and phenylpropanoid, were significantly different in *sitcd1* compared to WT and *SiTCD1*-OE (Appendix L). Surprisingly, the transcription levels of most genes related to metabolic pathways required for ATP energy were significantly down-regulated in *sitcd1* under L20/D18 conditions (Fig. 5-C). The results of qRT-PCR and RNA-seq agreed. The relative expression levels of multiple metabolism genes were significantly reduced in *sitcd1*, such as *psaA*, *rbcL*, and *HEMA* involved in porphyrin and chlorophyll metabolism; *ATP-PFK7*, *G6PI*, and *GH17* involved in starch and sucrose metabolism; *PEPC1*, *PEPC2*, and *MDH2* involved in carbon metabolism; and *APX2*, *GSTZ5*, and *GST23* involved in glutathione metabolism (Fig. 5-D). In addition, there were significant differences between *sitcd1* and WT in the transcription levels of cold-regulated genes, such as *CBF*, *COLD1*, and *ICE1*, but not between *sitcd1* and *SiTCD1*-OE (Fig. 5-C and D) (Appendix M).

Consistent with the transcription levels above, the ATP content of energy suppliers sharply decreased (Fig. 5-E), leading to declines in chlorophyll and soluble sugar content (SSC) (Appendix M) in *sitcd1* at L20/D18. Note that the content of reactive oxygen species (ROS) was higher in *sitcd1* compared to the WT and transgenic lines (Appendix M). Although the GR enzyme activity was higher in *sitcd1* than in WT and *SiTCD1*-OE, GSH and its redox couple (GSH/GSSG) were lower (Fig. 5-E). These results indicated that SiTCD1 not only influences the optimal expression of plastid genes but also the genes related to the metabolic consumption of ATP in seedlings under low temperatures in foxtail millet.

3.9. Haplotype analysis of *SiTCD1*

To determine the nucleotide variations of *SiTCD1*, the genomic sequence of *SiTCD1* was analyzed in a 110 *Setaria* pan-genome and 11 haplotypes were identified. Among them, *Hap3* to *Hap11* were mainly found in wild accessions. While Hap1 and Hap2 were mainly found in foxtail millet accessions, there was only one variation between them, a 349 bp insertion at 750 bp upstream of the start codon (ATG) in the promoter region of *SiTCD1* (Fig. 6-A). Based on the variation between *Hap1* and *Hap2*, the molecular marker *Pro-1* was developed to genotype the foxtail millet accessions into two haplotypes, namely $SiTCD1^{Hap1}$ (*Hap1*) and $SiTCD1^{Hap2}$ (*Hap2*).

To catalog the natural variation at *SiTCD1* in foxtail millet germplasm, a haplotype analysis was performed on 195 foxtail millet accessions (141 Chinese landraces, 47 modern cultivars, and seven worldwide landraces) using the *Pro-1* marker. The distribution of haplotypes in those accessions was characterized as: *Hap1* in 126 Chinese landraces, 42 modern cultivars, and seven worldwide landraces; and *Hap2* in 15 Chinese landraces and five modern cultivars (Appendix N). In total, 1.5% of the southern landraces or cultivars harbored *Hap2*, while 14.2% of the northern landraces or cultivars harbored *Hap2*, but regardless of the southern or northern distinction, accessions carrying *Hap2* were less numerous than those carrying *Hap1* (Fig. 6-B). However, most accessions (94.1%) in *Hap2* were northern landraces or cultivars (Fig. 6-C). Given that *sitcd1* was more sensitive at the bud bursting stage than the germination and seedling stages under cold stress (Appendix O), the cold tolerance level of the 195 accessions was evaluated under cold stress treatment at the bud bursting stage by a weighted aggregation of different levels (Appendix P). The cold tolerance of accessions carrying the *Hap2* allele was significantly higher than those with the *Hap1* allele, whereas their growth was comparable under normal conditions (Fig. 6-D). The *SiTCD1* expression levels in leaves from five randomly chosen accessions with the *Hap1* allele were significantly lower than those from five randomly chosen varieties with the *Hap2* allele under cold stress conditions, but not under normal temperatures (Fig. 6-E).

4. Discussion

4.1. *SiTCD1* is essential for early chloroplast development in foxtail millet

The PPR proteins are involved in RNA metabolism *via* cleavage, splicing, editing, and the modulation of RNA stability, and they are vital for chloroplast development in plants (Tillich and Krause 2010; Barkan 2011). Unlike the well-studied PPRs in *Arabidopsis* and rice, the functions of PPRs in foxtail millet remain largely unexplored. In the current study, we cloned *SiTCD1*, which encodes a PPR protein, by using the mutant *sitcd1*. SiTCD1 is homologous to AtMEE40 (Zybailov *et al.* 2008) and OsYSA (Su *et al.* 2012), and it has a predicted cTP and is located in the chloroplasts. The AtMEE40 mutant had not been identified previously. The absence of five PPR motifs in OsYSA is responsible for the *ysa* mutant, which has albino leaves before the three-leaf stage. However, its temperature-sensitivity characteristics and molecular regulatory mechanisms under different temperatures had not been reported (Su *et al.* 2012). In this study, *sitcd1* exhibited normal green leaves under high temperatures. Nevertheless, *sitcd1*, with an albino phenotype during early leaf development, was characterized by reduced chlorophyll contents and abnormal chloroplasts under low temperatures. The expression of *SiTCD1* was upregulated in response to low temperatures in all materials, and the transcription level of *SiTCD1* was not significantly different between WT and *sitcd1* (Fig. 2-G). However, the sitcd1 protein failed to enter the chloroplasts due to the absence of 68 aa at the N terminus of SiTCD1, which serve as a

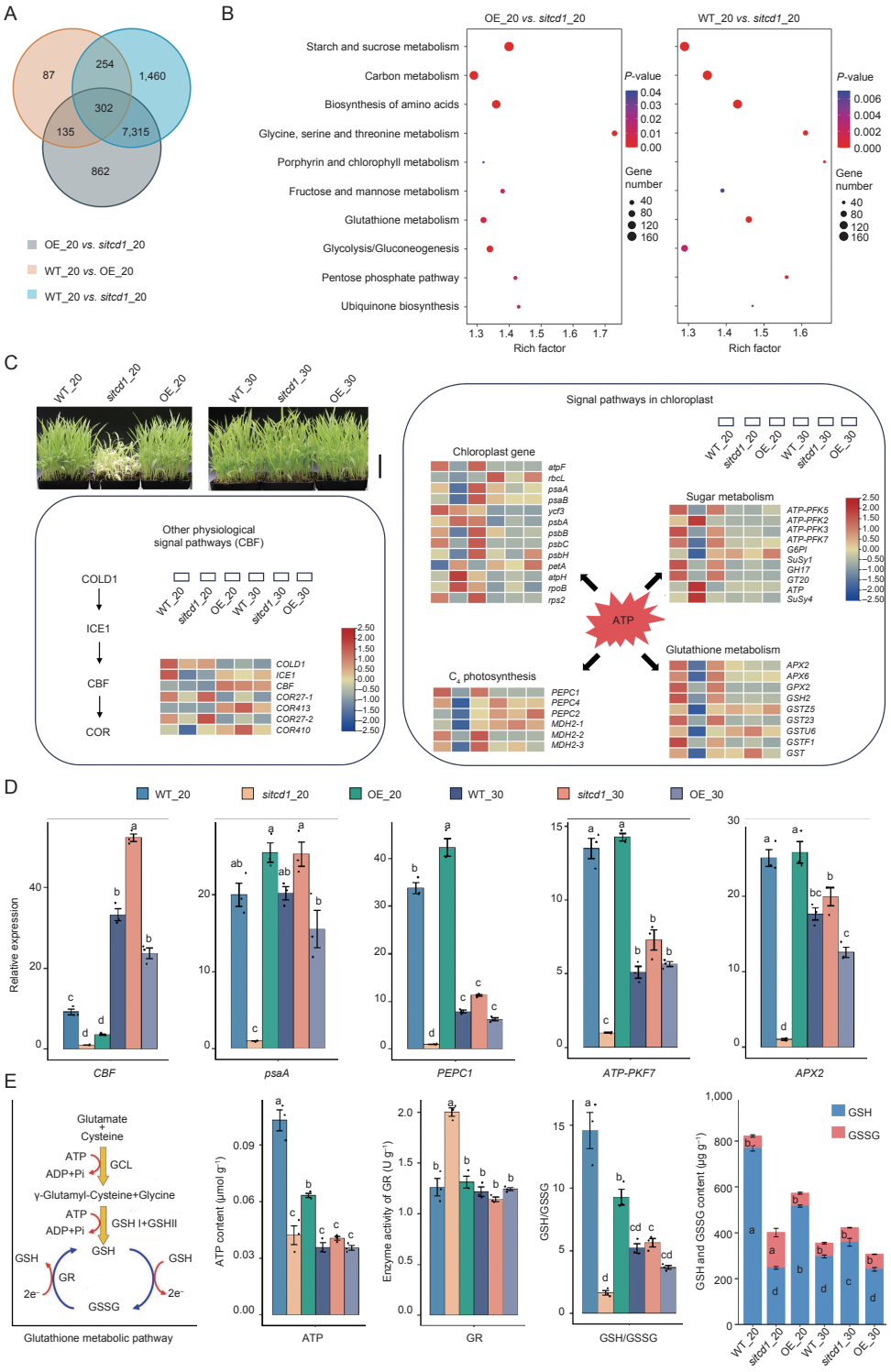


Fig. 5 RNA-seq analysis of wild type (WT), *sitcd1* and transgenic line (*SiTCD1*-OE) seedling leaves under L20/D18 and L30/D28 conditions. A, Venn diagram showing the overlap of differentially expressed genes (DEGs) among WT, *sitcd1* and overexpression (OE) at light/dark temperatures of 20°C/18°C (L20/D18) condition. B, Kyoto Encyclopedia of Genes and Genomes (KEGG) pathway analyses of WT *vs*. *sitcd1* and *SiTCD1*-OE *vs*. *sitcd1* at L20/D18. Gene numbers (circle size) and enrichment *P*-values (circle color) are shown. C, Heatmap of genes related to the ICE1-CBF-COR cold response and signal pathway in chloroplasts (porphyrin and chlorophyll metabolism, starch and sucrose metabolism, carbon metabolism, and glutathione metabolism) under L20/D18 and light/dark temperatures of 30°C/28°C (L30/D28) conditions. The phenotypic images in the upper left corner show the phenotypes of WT and *sitcd1* at the time of transcriptome sampling. Bar=3 cm. D, qRT-PCR validation of genes related to the ICE1-CBF-COR cold response and signaling pathway in chloroplast (chlorophyll metabolism, starch and sucrose metabolism, carbon metabolism and glutathione metabolism) among WT, *sitcd1* and OE at L20/D18 and L30/D28. E, glutathione metabolism related elements: ATP content, glutathione reductase (GR) enzymatic activity, reduced glutathione (GSH) and its redox couple (GSH/oxidized glutathione (GSSG)), as well as the contents of GSH and GSSG among WT, *sitcd1* and OE at L20/D18 and L30/D28. WT_20, *sitcd1*_20 and OE_20 represent the plants grown at L20/D18. WT_30, *sitcd1*_30 and OE_30 represent the plants grown at L30/D28. Bars mean SD (n=3). Letters indicate significant differences (P<0.01, one-way ANOVA, Duncan's test).

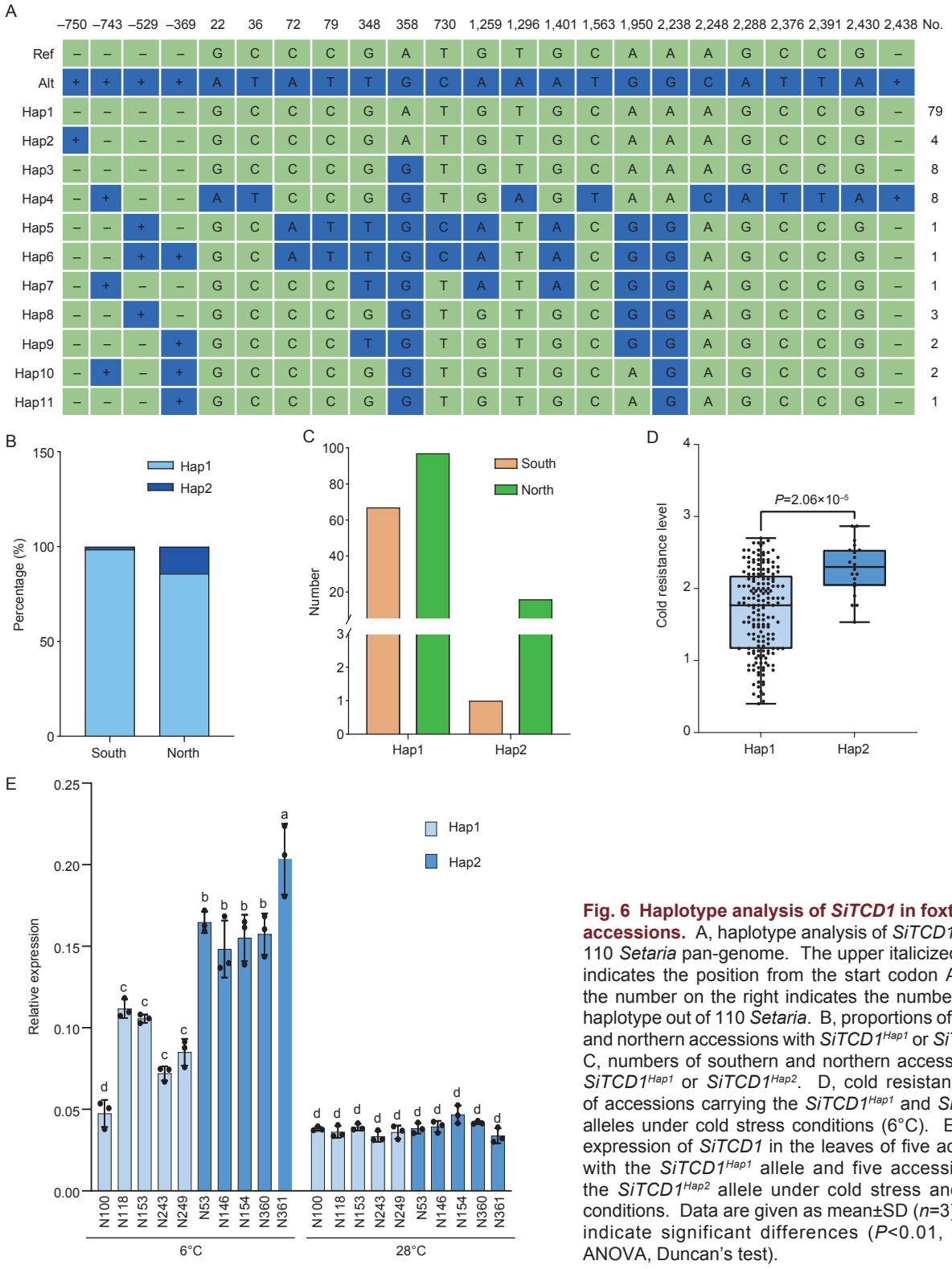


Fig. 6 Haplotype analysis of *SiTCD1* in foxtail millet accessions. A, haplotype analysis of *SiTCD1* from the 110 *Setaria* pan-genome. The upper italicized number indicates the position from the start codon ATG, and the number on the right indicates the number of each haplotype out of 110 *Setaria*. B, proportions of southern and northern accessions with $SiTCD1^{Hap1}$ or $SiTCD1^{Hap2}$. C, numbers of southern and northern accessions with $SiTCD1^{Hap1}$ or $SiTCD1^{Hap2}$. D, cold resistance levels of accessions carrying the $SiTCD1^{Hap1}$ and $SiTCD1^{Hap2}$ alleles under cold stress conditions (6°C). E, relative expression of *SiTCD1* in the leaves of five accessions with the $SiTCD1^{Hap1}$ allele and five accessions with the $SiTCD1^{Hap2}$ allele under cold stress and normal conditions. Data are given as mean±SD (n=3). Letters indicate significant differences (P<0.01, one-way ANOVA, Duncan's test).

chloroplast transit peptide (cTP) crucial for chloroplast targeting (Fig. 2-H–I). This mechanism is analogous to that of Pst_12806, which also requires a cTP to enter chloroplasts and influence their function (Xu *et al.* 2019). Consequently, we hypothesize that the mutated SiTCD1 cannot enter the chloroplasts to perform its functions, resulting in the observed phenotypes in *sitcd1* at low temperatures (Fig. 7).

4.2. The *SiTCD1* gene might be involved in *atpF* splicing at low temperatures

Seventeen introns (16 group II introns and one group I intron) were identified in the chloroplast genome of foxtail millet, and that number is similar to that in the rice chloroplast genome. Among those introns, we detected a higher level of the unspliced *atpF* transcripts, *atpF-U*, in *sitcd1* compared to WT under L20/D18 conditions. *atpF* encodes the CF_0I subunit of

chloroplast ATP synthase (cpATPase). Abnormal *atpF* intron splicing results in lower chloroplast ATP synthase activity in the *wsl4* and *ylws* mutants (Wang *et al.* 2017; Lan *et al.* 2023). Disrupting cpATPase function leads to the impairment of photosynthesis and the accumulation and assembly of photosynthetic complexes (Rühle *et al.* 2014). In addition, alternative splicing of pre-mRNA produces multiple splice isoforms from a single gene, each with distinct functions, and this plays a crucial role in regulating plant responses to cold. For instance, IDD14β, an alternatively spliced IDD14 form, may modulate starch accumulation in response to cold (Seo *et al.* 2011). The regulation of *CCA1* alternative splicing contributes to freezing tolerance since 35S:*CCA1α* transgenic lines showed enhanced freezing tolerance, while the 35S:*CCA1β* transgenic lines were sensitive to freezing (Seo *et al.* 2012). In our current study, *atpF-S* was markedly lower in *sitcd1*, whereas *atpF-U* was higher in *sitcd1* compared to the WT and transgenic lines at low temperatures. These findings indicated that the transcript of the atpF-S splice isoform is crucial for regulating chloroplast development at low temperatures. Despite the inability of mutant SiTCD1 to enter the chloroplast due to the absence of the cTP, a small quantity of *atpF-S* remained in *sitcd1* at low temperatures. We hypothesize that apart from SiTCD1, other RNA-binding proteins might participate in the splicing of the *atpF* intron during cold stress (Fig. 7).

4.3. Possible pathway by which *SiTCD1* regulates chloroplast development under low temperature conditions

Throughout evolution, plants have developed a mechanism for cold acclimation which involves transcriptional, post-transcriptional, and translational regulatory factors that trigger the expression of functional genes in response to low temperatures. The ICE1-CBF-COR signaling pathway has been the most well studied transcriptional pathway in this regard (Kopeć *et al.* 2022). In this study, no significant differences were observed between *sitcd1* and *SiTCD1*-OE at the transcriptional level of cold-regulated genes like *CBF*, *COLD1*, and *ICE1*. This indicates the presence of other signal transduction pathways for regulating the cold response.

The chloroplasts have been suggested to act as the central switch in the response to cold stress in plants. Cold conditions alter the metabolic consumption of ATP by the CBB cycle and other energy consuming processes (Gao *et al.* 2022). At low temperatures, the mutation of *SiTCD1* leads to a deficiency in the splice isoform *atpF-S*, thus significantly reducing ATP production. This ATP shortage hampers the activation of the rate-limiting enzyme glutamyl tRNA reductase, which is crucial for chlorophyll synthesis (Jahn 1992), resulting in the reduced chlorophyll content in *sitcd1*. In addition, cold stress disrupts cellular homeostasis, causing the accumulation of ROS in various organelles, particularly chloroplasts (Zu *et al.* 2023). GSH and GR scavenge ROS and its reaction products to provide tolerance to cold stress (Gill *et al.* 2013). WSL, a chloroplast-localized PPR protein, is involved in *rpl2* splicing and affects chloroplast development. Its mutant, *wsl*, shows significant ROS accumulation under abiotic stress in rice (Tan *et al.* 2014). Note that the content of ROS was also higher in *sitcd1* compared to the WT and transgenic lines under L20/D18 conditions in this study. Due to the insufficient ATP supply in *sitcd1*, GSH and its redox couple (GSH/GSSG) remained low despite the higher GR enzymatic activity. However, there were no manifest differences in the enzymatic activities of SOD and POD between *sitcd1* and WT and transgenic lines under L20/D18 condition, but there was a difference in CAT (Appendix M). Based on these findings, we speculate that the sensitivity of *sitcd1* to temperature is due to abnormal chlorophyll and glutathione metabolism caused by an inadequate ATP supply (Fig. 7).

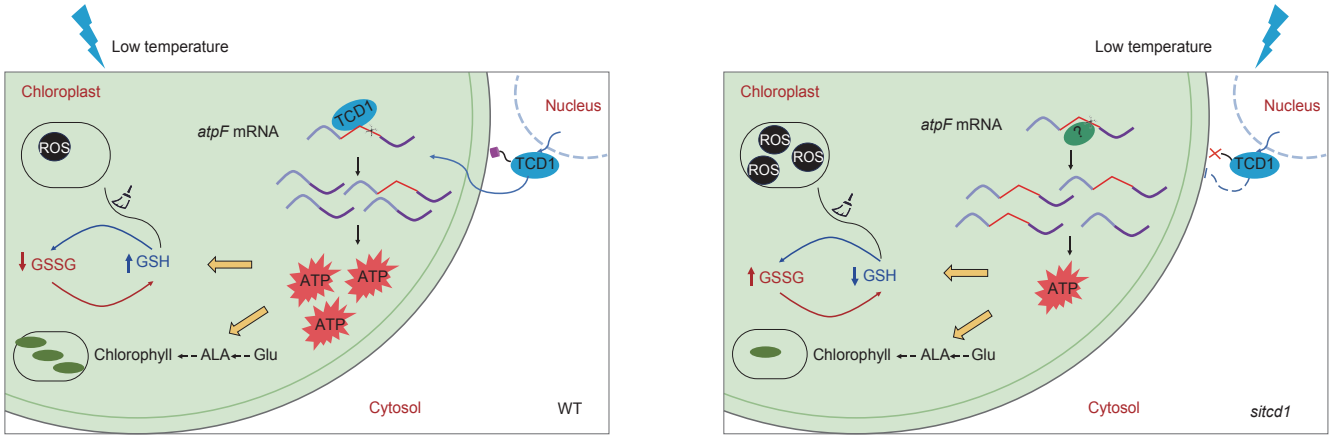


Fig. 7 A speculative working model depicting the molecular function of SiTCD1. The nuclear-encoded SiTCD1 is transported into the chloroplast *via* the cTP, where it plays a crucial role in regulating chloroplast gene expression at low temperatures. SiTCD1 directly modulates the intron splicing of *atpF* genes. At low temperatures, the transcript of splice isoform atpF-S from *atpF* is significantly reduced in *sitcd1* due to the inability of the SiTCD1 mutant to access the chloroplast, due to the absence of cTP. This leads to an ATP supply that is insufficient for chlorophyll synthesis and reduces the ability of reduced glutathione (GSH) to scavenge reactive oxygen species (ROS). Consequently, the seedlings exhibit an albino phenotype and the content of ROS is also higher in *sitcd1*. GSSG, oxidized glutathione; ALA, 5-aminolevulinic acid; Glu, glutamate.

Foxtail millet is a C_4 model plant with high CO_2 fixation efficiency (Yang *et al.* 2020) that serves as an ideal species for exploring the mechanisms involved in chloroplast development. The mutant *sistl2*, with lower transcription levels of C_4 photosynthesis-related genes, impacts C_4 photosynthetic capacity (Zhang *et al.* 2018). In the C_4 photosynthetic pathway, the conversion of pyruvate to phosphoenolpyruvate is an ATP energy dependent process (Ishikawa *et al.* 2016). In the present study, with higher C_i, lower P_n and abnormal Kranz structures, the transcription levels of C_4 photosynthesis-related genes (*PEPC1*, *PEPC2*, and *MDH2*) were significantly downregulated in *sitcd1*. Further investigation is needed to determine whether *SiTCD1* affects the CO_2 fixation efficiency and C_4 photosynthetic rate under cold stress.

4.4. Natural variants of *SiTCD1* related to cold tolerance in foxtail millet

The identification of natural variants for cold stress-related genes is crucial for the molecular breeding of spring foxtail millet. Natural variation at the *INDUCER OF CBF EXPRESSION 1* (*ZmICE1*) promoter determines the binding affinity with its transcriptional activator ZmMYB39, a positive regulator of cold tolerance in maize; resulting in different degrees of *ZmICE1* transcription and cold tolerance among inbred lines (Jiang *et al.* 2022). Here, the haplotypes of *SiTCD1* were investigated in 195 accessions and the associations of haplotypes with their cold tolerance levels were determined. The cold tolerance of the accessions carrying *Hap2* allele was found to be significantly higher than that of accessions with the *Hap1* allele at the bud bursting stage under cold stress. Only 10.3% of the 195 accessions harbored *Hap2*, which conferred higher tolerance to cold, indicating that the *Hap2* allele has not been well utilized for cold tolerance in foxtail millet. Meanwhile, a 349 bp insertion in *Hap2*, a MYB element, was predicted by PlantCARE (http://bioinformatics.psb.ugent.be/webtools/plantcare/html/). We speculate that variation at the *SiTCD1* promoter might explain the difference in cold tolerance observed between the two haplotypes. However, the underlying mechanism driving variation in the promoter in response to low temperature remains to be further studied.

5. Conclusion

During early leaf development in foxtail millet, the temperature-sensitive chlorophyll-deficient (*sitcd1*) mutation exhibits an albino phenotype characterized by reduced chlorophyll content and abnormal chloroplasts at low temperatures of 20°C during the day and 18°C at night. Map-based cloning showed that *SiTCD1* encodes a P-type PPR protein. SiTCD1 was found to bind directly to the plastid gene *atpF in vitro*, so it plays a role in the splicing of the *atpF* gene. Abnormal *atpF* splicing leads to reductions in chlorophyll content, GSH, and its redox couple (GSH/GSSG) in *sitcd1* at low temperatures. Accessions with the $SiTCD1^{Hap2}$ allele demonstrated greater tolerance to cold stress than those with the $SiTCD1^{Hap1}$ allele during the bud bursting stage. Thus, *SiTCD1* is essential for early chloroplast development, and this study offers valuable genetic resources for enhancing cold tolerance under low temperature conditions in foxtail millet.

Acknowledgements

This research was supported by the Central Guidance on Local Science and Technology Development Fund of Shanxi Province, China (YDZJSX2022A043), the Minor Crop Molecular Breeding Platform Special Project of Shanxi Academy of Agricultural Sciences, China (YGC2019FZ3), the Key R&D Projects of Shanxi Province, China (202102140601003), the Modern Agriculture Industry Technology System Construction Project of Shanxi Province, China (2024CYJSTX04-01), the Shanxi Province Agricultural Key Core Technology Research, China (NYGG19), and the Shanxi Province Science and Technology Innovation Team Project, China (2015013001-09).

Declaration of competing interest

The authors declare that they have no conflict of interest.

Declaration of enerative AI and AI-assisted technologies in the writing process

During the preparation of this manuscript, the authors used ChatGPT 4.0 to assist in improving the clarity and readability of the language. All content generated was carefully reviewed and revised by the authors as necessary, and the authors take full responsibility for the final content of the article.

Data availability

The RNA-seq data in this publication have been deposited in the SRA database of NCBI and are accessible through Series accession number PRJNA994700. The BSA-seq data in this publication have been deposited in the SRA database of NCBI and are accessible through Series accession number PRJNA997593.

Appendices associated with this paper are available at https://doi.org/10.1016/j.jia.2024.12.022

References

Abe A, Kosugi S, Yoshida K, Natsume S, Takagi H, Kanzaki H, Matsumura H, Yoshida K, Mitsuoka C, Tamiru M. 2012. Genome sequencing reveals agronomically important loci in rice using MutMap. *Nature Biotechnology*, **30**, 174–178.

Alpert A J, Gilbert H F. 1985. Detection of oxidized and reduced glutathione with a recycling postcolumn reaction. *Analytical Biochemistry*, **144**, 553–562.

Arnon D I. 1949. Copper enzymes in isolated chloroplasts. Polypheoloxidase in *Beta vulgaris*. *Plant Physiology*, **24**, 1–15.

Barkan A. 2011. Expression of plastid genes: Organelle-specific elaborations on a prokaryotic scaffold. *Plant Physiology*, **155**, 1520–1532.

Barkan A, Small I. 2014. Pentatricopeptide repeat proteins in plants. *Annual Review of Plant Biology*, **65**, 415–442.

Beutler E, Mathai C K. 1967. A comparison of normal red cell ATP levels as measured by the firefly system and the hexokinase system. *Blood*, **30**, 311–320.

Buysse J, Merckx R. 1993. An improved colorimetric method to quantify sugar content of plant tissue. *Journal of Experimental Botany*, **44**, 1627–1629.

Chen C Z, Wang Y L, He M X, Li Z W, Shen L, Li Q, Ren D Y, Hu J,

Zhu L, Zhang G H, Gao Z Y, Zeng D L, Guo L B, Qian Q, Zhang Q. 2023. OsPPR9 encodes a DYW-type PPR protein that affects editing efficiency of multiple RNA editing sites and is essential for chloroplast development. *Journal of Integrative Agriculture*, **22**, 972–980.

Chen L, Huang L H, Dai L P, Gao Y H, Zou W W, Lu X L, Wang C J, Zhang G H, Ren D Y, Hu J, Shen L, Dong G J, Gao Z Y, Chen G, Xue D W, Guo L B, Xing Y Z, Qian Q, Zhu L, Zeng D L. 2019. *PALE-GREEN LEAF12* encodes a novel pentatricopeptide repeat protein required for chloroplast development and 16S rRNA processing in rice. *Plant Cell Physiology*, **60**, 587–598.

Chen S B, Tao L Z, Zeng L R, Vega-Sanchez M E, Umemura K, Wang G L. 2006. A highly efficient transient protoplast system for analyzing defence gene expression and protein-protein interactions in rice. *Molecular Plant Pathology*, **7**, 417–427.

Cui X A, Wang Y W, Wu J X, Han X, Gu X F, Lu T G, Zhang Z G. 2019. The RNA editing factor DUA1 is crucial to chloroplast development at low temperature in rice. *New Phytologist*, **221**, 834–849.

Demiral T, Türkan I. 2005. Comparative lipid peroxidation, antioxidant defense systems and proline content in roots of two rice cultivars differing in salt tolerance. *Environmental and Experimental Botany*, **53**, 247–257.

Fang X M, Dong K J, Wang X Q, Liu T P, He J H, Ren R Y, Zhang L, Liu R, Liu X Y, Li M, Huang M Z, Zhang Z S, Yang T Y. 2016. A high density genetic map and QTL for agronomic and yield traits in Foxtail millet [*Setaria italica* (L.) P. Beauv]. *BMC Genomics*, **17**, 336.

Gao Y, Thiele W, Saleh O, Scossa F, Arabi F, Zhang H, Sampathkumar A, Kühn K, Fernie A, Bock R, Schöttler M A, Zoschke R. 2022. Chloroplast translational regulation uncovers nonessential photosynthesis genes as key players in plant cold acclimation. *Plant Cell*, **34**, 2056–2079.

Gill S S, Anjum N A, Hasanuzzaman M, Gill R, Trivedi D K, Ahmad I, Pereira E, Tuteja N. 2013. Glutathione and glutathione reductase: A boon in disguise for plant abiotic stress defense operations. *Plant Physiology and Biochemistry*, **70**, 204–212.

He Q, Tang S, Zhi H, Chen J F, Zhang J, Liang H K, Alam O, Li H B, Zhang H, Xing L H, Li X K, Zhang W, Wang H L, Shi J P, Du H L, Wu H P, Wang L W, Yang P, Xing L, Yan H S, *et al.* 2023. A graph-based genome and pan-genome variation of the model plant *Setaria*. *Nature Genetics*, **55**, 1232–1242.

Ishikawa N, Takabayashi A, Sato F, Endo T. 2016. Accumulation of the components of cyclic electron flow around photosystem I in C_4 plants, with respect to the requirements for ATP. *Photosynthesis Research*, **129**, 261–277.

Jahn D. 1992. Complex formation between glutamyl-tRNA synthetase and glutamyl-tRNA reductase during the tRNA-dependent synthesis of 5-aminolevulinic acid in *Chlamydomonas reinhardtii*. *FEBS Letters*, **314**, 77–80.

Jia X P, Zhang Z B, Liu Y H, Zhang C W, Shi Y S, Song Y C, Wang T Y, Li Y. 2009. Development and genetic mapping of SSR markers in foxtail millet [*Setaria italica* (L.) P. Beauv.]. *Theoretical and Applied Genetics*, **118**, 821–829.

Jiang H F, Shi Y T, Liu J Y, Li Z, Fu D Y, Wu S F, Li M Z, Yang Z J, Shi Y L, Lai J S, Yang X H, Gong Z Z, Hua J, Yang S H. 2022. Natural polymorphism of *ZmICE1* contributes to amino acid metabolism that impacts cold tolerance in maize. *Nature Plants*, **8**, 1176–1190.

Kopeć P, Rapacz M, Arora R. 2022. Post-translational activation of CBF for inducing freezing tolerance. *Trends in Plant Science*, **27**, 415–417.

Lan J, Lin Q B, Zhou C L, Liu X, Miao R, Ma T F, Chen Y P, Mou C L, Jing R N, Feng M, Nguyen T, Ren Y L, Cheng Z J, Zhang X, Liu S J, Jiang L, Wan J M. 2023. *Young Leaf White Stripe* encodes a P-type PPR protein required for chloroplast development. *Journal of Integrative Plant Biology*, **65**, 1687–1702.

Li H, Durbin R. 2009. Fast and accurate short read alignment with Burrows-Wheeler transform. *Bioinformatics*, **25**, 1754–1760.

Li H, Handsaker B, Wysoker A, Fennell T, Ruan J, Homer N, Marth G, Abecasis G, Durbin R. 2009. The sequence alignment/map format and SAMtools. *Bioinformatics*, **25**, 2078–2079.

Li J H, Zhang Z Y, Chong K, Xu Y Y. 2022. Chilling tolerance in rice: Past and present. *Journal of Plant Physiology*, **268**, 153576.

Li J Y, Yang C, Tian Y Y, Liu J X. 2022. Regulation of chloroplast development and function at adverse temperatures in plants. *Plant Cell Physiology*, **63**, 580–591.

Li W, Tang S, Zhang S, Shan J G, Tang C J, Chen Q N, Jia G Q, Han Y H, Zhi H, Diao X M. 2016. Gene mapping and functional analysis of the novel leaf color gene *SiYGL1* in foxtail millet [*Setaria italica* (L.) P. Beauv]. *Physiologia Plantarum*, **157**, 24–37.

Li X K, Gao J H, Song J Y, Guo K, Hou S Y, Wang X C, He Q, Zhang Y Y, Zhang Y K, Yang Y L, Tang J Y, Wang H L, Persson S, Huang M Q, Xu L S, Zhong L L, Li D Q, Liu Y M, Wu H, Diao X M, *et al.* 2022. Multi-omics analyses of 398 foxtail millet accessions reveal genomic regions associated with domestication, metabolite traits, and anti-inflammatory effects. *Molecular Plant*, **15**, 1367–1383.

Liu J M, Xu Z S, Lu P P, Li W W, Chen M, Guo C H, Ma Y Z. 2016. Genome-wide investigation and expression analyses of the pentatricopeptide repeat protein gene family in foxtail millet. *BMC Genomics*, **17**, 840.

Liu X, Lan J, Huang Y S, Cao P H, Zhou C L, Ren Y K, He N Q, Liu S J, Tian Y L, Nguyen T, Jiang L, Wan J M. 2018. WSL5, a pentatricopeptide repeat protein, is essential for chloroplast biogenesis in rice under cold stress. *Journal of Experimental Botany*, **69**, 3949–3961.

Liu X Y, Zhang X C, Cao R J, Jiao G A, Hu S K, Shao G N, Sheng Z H, Xie L H, Tang S Q, Wei X J, Hu P S. 2021. *CDE4* encodes a pentatricopeptide repeat protein involved in chloroplast RNA splicing and affects chloroplast development under low-temperature conditions in rice. *Journal of Integrative Plant Biology*, **63**, 1724–1739.

Mckenna A, Hanna M, Banks E, Sivachenko A, Cibulskis K, Kernytsky A, Garimella K, Altshuler D, Gabriel S, Daly M. 2010. The genome analysis toolkit: A MapReduce framework for analyzing next-generation DNA sequencing data. *Genome Research*, **20**, 1297–1303.

Okuzaki A, Ruhle T, Leister D, Schmitz-Linneweber C. 2021. The acidic domain of the chloroplast RNA-binding protein CP31A supports cold tolerance in *Arabidopsis thaliana*. *Journal of Experimental Botany*, **72**, 4904–4914.

Pfalz J, Bayraktar O A, Prikryl J, Barkan A. 2009. Site-specific binding of a PPR protein defines and stabilizes 5′ and 3′ mRNA termini in chloroplasts. *EMBO Journal*, **28**, 2042–2052.

Rühle T, Razeghi J A, Vamvaka E, Viola S, Gandini C, Kleine T, Schünemann D, Barbato R, Jahns P, Leister D. 2014. The Arabidopsis protein CONSERVED ONLY IN THE GREEN LINEAGE160 promotes the assembly of the membranous part of the chloroplast ATP synthase. *Plant Physiology*, **165**, 207–226.

Seo P J, Kim M J, Ryu J Y, Jeong E Y, Park C M. 2011. Two splice variants of the IDD14 transcription factor competitively form nonfunctional heterodimers which may regulate starch metabolism. *Nature Communications*, **2**, 303.

Seo P J, Park M J, Lim M H, Kim S G, Lee M, Baldwin I T, Park C M. 2012. A self-regulatory circuit of CIRCADIAN CLOCK-ASSOCIATED1 underlies the circadian clock regulation of temperature responses in *Arabidopsis*. *Plant Cell*, **24**, 2427–2442.

Su N, Hu M L, Wu D X, Wu F Q, Fei G L, Lan Y, Chen X L, Shu X L, Zhang X, Guo X P, Cheng Z J, Lei C L, Qi C K, Jiang L, Wang H, Wan J M. 2012. Disruption of a rice pentatricopeptide repeat protein causes a seedling-specific albino phenotype and its utilization to enhance seed purity in hybrid rice production. *Plant Physiology*, **159**, 227–238.

Tan J J, Tan Z H, Wu F Q, Sheng P K, Heng Y Q, Wang X H, Ren Y L, Wang J L, Guo X P, Zhang X, Cheng Z J, Jiang L, Liu X M, Wang H Y, Wan J M. 2014. A novel chloroplast-localized pentatricopeptide repeat protein involved in splicing affects chloroplast development and abiotic stress response in rice. *Molecular Plant*, **7**, 1329–1349.

Tang C J, Tang S, Zhang S, Luo M Z, Jia G Q, Zhi H, Diao X M. 2019. *SiSTL1*, encoding a large subunit of ribonucleotide reductase, is crucial for plant growth, chloroplast biogenesis, and cell cycle progression in *Setaria italica*. *Journal of Experimental Botany*, **70**, 1167–1182.

Tillich M, Krause K. 2010. The ins and outs of editing and splicing of plastid RNAs: Lessons from parasitic plants. *Nature Biotechnology*, **27**, 256–266.

Wang S, Bai G, Wang S, Yang L Y, Yang F, Wang Y, Zhu J K, Hua J. 2016. Chloroplast RNA-binding protein RBD1 promotes chilling tolerance through 23S rRNA processing in *Arabidopsis*. *PLoS Genetics*, **12**, e1006027.

Wang Y, Ren Y L, Zhou K N, Liu L L, Wang J L, Xu Y, Zhang H, Zhang

L, Feng Z M, Wang L W, Ma W W, Wang Y L, Guo X P, Zhang X, Lei C L, Cheng Z J, Wan J M. 2017. *WHITE STRIPE LEAF4* encodes a novel P-type PPR protein required for chloroplast biogenesis during early leaf development. *Frontiers in Plant Science*, **8**, 1116.

Wang Y F, Zhang J H, Shi X L, Peng Y, Li P, Lin D Z, Dong Y J, Teng S. 2016. Temperature-sensitive albino gene *TCD5*, encoding a monooxygenase, affects chloroplast development at low temperatures. *Journal of Experimental Botany*, **67**, 5187–5202.

Xu Q, Tang C L, Wang X D, Sun S T, Zhao J R, Kang Z S, Wang X J. 2019. An effector protein of the wheat stripe rust fungus targets chloroplasts and suppresses chloroplast function. *Nature Communications*, **10**, 5571.

Yan J J, Yao Y Y, Hong S X, Yang Y, Shen C C, Zhang Q X, Zhang D L, Zou T T, Yin P. 2019. Delineation of pentatricopeptide repeat codes for target RNA prediction. *Nucleic Acids Research*, **47**, 3728–3738.

Yang Z R, Zhang H S, Li X K, Shen H M, Gao J H, Hou S Y, Zhang B, Mayes S, Bennett M, Ma J X, Wu C Y, Sui Y, Han Y H, Wang X C. 2020. A mini foxtail millet with an *Arabidopsis*-like life cycle as a C_4 model system. *Nature Plants*, **6**, 1167–1178.

Zhang L, Chen J L, Zhang L Q, Wei Y, Li Y J, Xu X Y, Wu H, Yang Z N, Huang J R, Hu F H, Huang W H, Cui Y L. 2021. The pentatricopeptide repeat protein EMB1270 interacts with CFM2 to splice specific group II introns in *Arabidopsis* chloroplasts. *Journal of Integrative Plant Biology*, **63**, 1952–1966.

Zhang L, Zhou W, Che L P, Rochaix J D, Lu C M, Li W J, Peng L W. 2019. PPR protein BFA2 is essential for the accumulation of the *atpH/F* transcript in chloroplasts. *Frontiers in Plant Science*, **10**, 446.

Zhang S, Tang C J, Zhao Q, Li J, Yang L F, Qie L F, Fan X K, Li L, Zhang N, Zhao M C, Liu X T, Chai Y, Zhang X, Wang H L, Li Y T, Li W, Zhi H, Jia G Q, Diao X M. 2014. Development of highly polymorphic simple sequence repeat markers using genome-wide microsatellite variant analysis in Foxtail millet [*Setaria italica* (L.) P. Beauv.]. *BMC Genomics*, **15**, 78.

Zhang S, Tang S, Tang C J, Luo M Z, Jia G Q, Zhi H, Diao X M. 2018. SiSTL2 is required for cell cycle, leaf organ development, chloroplast biogenesis, and has effects on C_4 photosynthesis in *Setaria italica* (L.) P. Beauv. *Frontiers in Plant Science*, **9**, 1103.

Zhao Y N, Luo L L, Xu J S, Xin P Y, Guo H Y, Wu J, Bai L, Wang G G, Chu J F, Zuo J R. 2018. Malate transported from chloroplast to mitochondrion triggers production of ROS and PCD in *Arabidopsis thaliana*. *Cell Research*, **28**, 448–461.

Zhu Y J, Wu W J, Shao W, Chen J L, Shi X N, Ma X Y, Xu Y Z, Huang W H, Huang J R. 2020. SPLICING FACTOR1 is important in chloroplast development under cold stress. *Plant Physiology*, **184**, 973–987.

Zoschke R, Kroeger T, Belcher S, Schöttler M A, Barkan A, Schmitz-Linneweber C. 2012. The pentatricopeptide repeat-SMR protein ATP4 promotes translation of the chloroplast *atpB*/*E* mRNA. *The Plant Journal*, **72**, 547–558.

Zu X F, Luo L L, Wang Z, Gong J, Yang C, Wang Y, Xu C H, Qiao X H, Deng X, Song X W, Chen C, Tan B C, Cao X F. 2023. A mitochondrial pentatricopeptide repeat protein enhances cold tolerance by modulating mitochondrial superoxide in rice. *Nature Communications*, **14**, 6789.

Zybailov B, Rutschow H, Friso G, Rudella A, Emanuelsson O, Sun Q, van Wijk K J. 2008. Sorting signals, N-terminal modifications and abundance of the chloroplast proteome. *PLoS ONE*, **3**, e1994.

Executive Editor-in-Chief Xueyong Zhang
Managing Editor Ning Wang